Triple Differential Cross sections and Nuclear Recoil in Two-Photon Double Ionization of Helium

D. A. Horner,[1] C. W. McCurdy,[2,3] and T. N. Rescigno[2]

[1]*Los Alamos National Laboratory, Theoretical Division, Los Alamos, NM 87545*
[2]*Lawrence Berkeley National Laboratory, Chemical Sciences, Berkeley, CA 94720*
[3]*Departments of Applied Science and Chemistry, University of California, Davis, CA 95616*

(Dated: November 11, 2008)

Triple differential cross sections (TDCS) for two-photon double ionization of helium are calculated using the method of exterior complex scaling both above and below the threshold for sequential ionization (54.4 eV). It is found that sequential ionization produces characteristic behavior in the TDCS that identifies that process when it is in competition with nonsequential ionization. Moreover we see the signature in the TDCS and nuclear recoil cross sections of "virtual sequential ionization" below the threshold for the sequential process.

PACS numbers: 32.80.Fb, 32.80.Rm

I. INTRODUCTION

Double ionization of the helium atom by two XUV photons in the range of 40 to 50 eV has become the subject of intense theoretical interest in recent years [1–13] as well as the target of new experiments with high harmonic generation sources [14] and the first of a series of experiments underway at the free-electron laser source (FLASH) in Hamburg [15, 16]. The advent of new high intensity free-electron laser [17] and high-harmonic generation [18] light sources that operate in the VUV and soft X-ray regimes are on the verge of enabling kinematically complete experiments on this fundamental system.

To date, kinematically complete experiments (experiments in which the angular distributions and energies of both ejected electrons are detected) have been performed only for double ionization by a *single* XUV photon of simple atoms [19] and molecules [20]. However, these experiments, coupled with accurate *ab initio* theoretical calculations, have already yielded new understanding of electron correlation and its role in the double ionization process.

In the case of two-photon double ionization such experiments have yet to appear, but it is clear that they are on the horizon. These experiments will probe the role of electron correlation in both nonsequential ionization, where it is expected to play a central role, and sequential ionization, in which it is expected to be less important. It is in the completely differential quantity, the triple differential cross section (TDCS), that the electron correlation effects are most clearly revealed, and we will therefore focus much of our attention on those cross sections here.

Recently we reported total cross sections [21] for this process up to photon energies of 54.4 eV, the threshold of sequential double ionization and also reported single differential cross sections for energies up to 58 eV. In that work we predicted an effect that we can call "virtual sequential ionization" in which an indication of the onset of the sequential ionization process is seen in both the total cross section and the single differential cross section (SDCS or "energy-sharing cross section") well below the energetic threshold for that process. In the SDCS above threshold there are broad peaks centered at photoelectron energies corresponding to sequential ionization, and the wings of those peaks appear even at photon energies below that threshold (54.4 eV).

We have also reported the nuclear recoil cross sections [22], which derives from the TDCS, at energies above and below the sequential threshold, because this quantity is easier to measure than the TDCS, and in the absence of kinematically complete experiments it is likely to be the first differential quantity associated with two-photon double ionization to be well resolved. In fact, an encouraging recent measurement has been made at the FLASH facility, albeit not yet with high resolution [16].

The TDCS for two-photon double ionization is intrinsically different from that for one-photon double ionization. In the one-photon case, the ejection of two electrons is a process that occurs primarily because of the correlated motion of the two electrons. In the two-photon case, even below the sequential threshold, one can postulate a contribution to double photoionization in which each electron effectively absorbs the energy of one photon and the two electrons also interact with each other to produce the double ionization event. Electron correlation, while still essential to the process, is somewhat less important and is reflected in different ways in the angular distributions of the ejected electrons.

In this work we will explore both the general features and the details of those angular distributions in converged calculations using the method of exterior complex scaling (ECS) in a time-independent approach to the problem. We find that below the sequential threshold the TDCS has a shape that can be understood qualitatively as a modification by electron correlation of the angular distribution that would have been expected for sequential ejection of the electrons. When one electron is ejected nearly perpendicular to the polarization direction that modification of the simple pattern is extreme, and the effects of electron correlation create a more complicated

ejection pattern for the other than in the cases where one electron goes out close to the direction of polarization. The complete story of how electron correlation is reflected in these cross sections is only seen when these effects are examined as a function of the energy sharing between the two outgoing electrons.

We will begin here by summarizing the theoretical approach and its numerical implementation in Section II, where we will also discuss the convergence of the TDCS. In Section III we will present results for the total cross section in comparison with the results of other methods and explore the SDCS for a range of energies just above and below the sequential threshold. We will then turn to a survey of the TDCS and its interpretation. Finally, we present nuclear recoil cross sections for cuts of the momentum plane and for particular energy sharings, that are more detailed than the completely integrated nuclear recoil cross sections presented previously [22]. A summary and some concluding remarks are given in Section IV.

II. THEORY

A. Exterior Complex Scaling formulation of two photon absorption

We begin with the definition of the cross section for two-photon double ionization of an atom in terms of the ionization amplitude, $f(\mathbf{k}_1, \mathbf{k}_2, \omega)$,

$$\frac{d\sigma}{dE_1 d\Omega_1 d\Omega_2} = \frac{2\pi}{\hbar}\frac{(2\pi\alpha)^2}{m^2\omega^2} k_1 k_2 |f(\mathbf{k}_1, \mathbf{k}_2, \omega)|^2 \,, \qquad (1)$$

where $\mathbf{k}_1$ and $\mathbf{k}_2$ are the momenta of the photoelectrons, ω is the photon frequency, m is the electron mass and α is the fine-structure constant. The amplitude in Eq.(1) is the velocity form of the double photoionization amplitude,

$$f(\mathbf{k}_1, \mathbf{k}_2, \omega) = \langle \Psi^-_{\mathbf{k}_1,\mathbf{k}_2} | \mu [E_0 + \hbar\omega - H + i\epsilon]^{-1} \mu | \Phi_0 \rangle \,, \quad (2)$$

where H is the atomic Hamiltonian, Φ_0 is the initial state of the atom with corresponding energy E_0, and $\Psi^-_{\mathbf{k}_1,\mathbf{k}_2}$ is the full momentum-normalized scattering wave function, with incoming boundary conditions corresponding to two free electrons. For polarization $\boldsymbol{\epsilon}$, the dipole operator in the velocity form, μ, is defined in terms of the momentum operators, $\mathbf{p}_i$, for the two electrons by $\mu = \boldsymbol{\epsilon}\cdot\mathbf{p}_1 + \boldsymbol{\epsilon}\cdot\mathbf{p}_2$.

To formulate this problem using the ECS approach, we begin with the coupled driven equations in the Dalgarno-Lewis form of second order perturbation theory [23] that describe the absorption of two photons by a system initially in state Φ_0,

$$(E_0 + \hbar\omega - H)\Psi^{\rm sc}_1(\mathbf{r}_1, \mathbf{r}_2) = \mu\Phi_0 \qquad (3)$$

$$(E_0 + 2\hbar\omega - H)\Psi^{\rm sc}_2(\mathbf{r}_1, \mathbf{r}_2) = \mu\Psi^{\rm sc}_1 \,, \qquad (4)$$

which must be solved with pure outgoing wave boundary conditions for the wave functions $\Psi^{\rm sc}_1$ and $\Psi^{\rm sc}_2$. The two-photon double ionization amplitude is formally contained (to within an overall phase) in the asymptotic form of the solution of the second equation.

It is common in time-dependent calculations to extract double ionization cross sections by projecting a wave packet onto an approximation to the two-electron final continuum state, thereby defining an apparent rate for double ionization, as explained for example in refs. [3] and [24]. However, for time-independent descriptions of Coulomb breakup processes there is a long literature, going back to the foundational papers of Rudge, Seaton and Peterkop[25–27], deriving integral expressions for the ionization amplitude directly, without approximating the final state. In this approach one begins with the asymptotic form of the wave function, in our case $\Psi^{\rm sc}_2$, in the Coulomb three-body breakup channel,

$$\Psi^{\rm sc}_2 \underset{\rho\to\infty}{\longrightarrow} \sqrt{2\pi i}\left(\frac{K^3}{\rho^5}\right)^{1/2} e^{iK\rho + \zeta \ln 2K\rho + i\sigma_0} f(\mathbf{k}_1, \mathbf{k}_2, \omega) \qquad (5)$$

where $\rho = \sqrt{r_1^2 + r_2^2}$, which defines the amplitude for double ionization, $f(\mathbf{k}_1, \mathbf{k}_2, \omega)$. Applying the original ideas of Rudge [25] to a wave function known exactly in a large but finite volume, we have previously shown [28] that the double ionization amplitude can be extracted (to within an irrelevant volume-dependent overall phase) using a surface integral that involves a pair of testing functions, $\psi^-_{\mathbf{k}}(\mathbf{r})$, which are momentum-normalized, one-electron Coulomb functions with nuclear charge Z=2, in the case of helium:

$$f(\mathbf{k}_1, \mathbf{k}_2, \omega) = \frac{1}{2}\int \big(\psi^{-*}_{\mathbf{k_1}}(\mathbf{r_1})\psi^{-*}_{\mathbf{k_2}}(\mathbf{r_2})\,\nabla\,\Psi^{\rm sc}_2(\mathbf{r}_1, \mathbf{r}_2) - \Psi^{\rm sc}_2(\mathbf{r}_1, \mathbf{r}_2)\,\nabla\,\psi^{-*}_{\mathbf{k_1}}(\mathbf{r_1})\psi^{-*}_{\mathbf{k_2}}(\mathbf{r_2})\big)\cdot d\mathbf{S} \qquad (6)$$

It is important to note that, as discussed in detail previously [29–31], the functions $\psi^-_{\mathbf{k_1}}(\mathbf{r_1})$ and $\psi^-_{\mathbf{k_2}}(\mathbf{r_2})$ do *not* describe the final state of the system, but are merely the testing functions that extract the double ionization amplitude from from the asymptotic behavior of $\Psi^{\rm sc}_2$ via the surface integral in Eq.(6). No approximation concerning the final state has been made in this formalism, and electron correlation is treated completely in the final outgoing wavefunction $\Psi^{\rm sc}_2$ as well as in the initial state Φ_0 in this approach.

Now we proceed to solve Eqs. (3) and (4) using the ECS approach to impose the correct boundary conditions. In the ECS method we first scale the radial coordinates of both electrons by a complex phase factor outside a fixed radius, R_0,

$$r \to \begin{cases} r & r \le R_0 \\ R_0 + (r - R_0)e^{i\eta} & r > R_0 \end{cases} \qquad (7)$$

where R_0 defines the radius within which the wave function will be the usual function of real-valued coordinates,

and η is a scaling angle. In an exact or converged calculation the solutions of the Schrödinger equation for $r < R_0$ do not depend on η or R_0. As has been discussed elsewhere [28, 29, 32, 33] setting $\eta \neq 0$ effectively imposes outgoing scattering boundary conditions on both wave functions in Eqs. (3) and (4) if *on the complex contour* we require only that $\Psi \to 0$ as $r \to \infty$.

However, in those applications of the ECS method the right hand side of the relevant driven Schrödinger equation was square integrable, and the application of the correct boundary condition by the ECS transformation was therefore independent of the choice of R_0 as long as it was chosen to lie beyond the range of the driving function. In this application we have to address another problem. For photon energies exceeding the first ionization potential of the atom, the solution of Eq. (3) $\Psi_1^{\rm sc}$, will have single ionization terms that behave, at large *real* values of the electron coordinates, as the (symmetrized) product of a bound state of He^+ times an undamped outgoing wave in the other electron coordinate. This fact means that $\mu\Psi_1^{\rm sc}$, which is the driving term for Eq. (4), will not vanish as r_1 or $r_2 \to \infty$ along the real axis.

Because the dipole operator μ is a one-body operator, the application of outgoing boundary conditions via the ECS transformation in Eq. (4) will depend on the value of R_0, *irrespective of the gauge being used*, and the ionization amplitudes extracted from $\Psi_2^{\rm sc}$ will not converge with increasing volume of the space on which it is solved. We can circumvent this problem by adding a small, positive imaginary part to ω in Eq. (3) only, which will produce a solution $\Psi_1^{\rm sc}$ with an exponential fall-off for real r-values. With this procedure, we have a valid driving term for the solution of Eq. (4), which can then be solved directly under ECS for real ω. As we will see, this procedure yields convergent amplitudes that must then be numerically extrapolated to purely real photon energies. That extrapolation will be discussed in the following section on the numerical implementation of ECS for this problem.

B. Numerical implementation

In these calculations we have used the numerical procedures and the representation of the wave functions previously utilized for both the H^- anion [34] and molecular hydrogen [35] and decompose the full scattered wave into angular components on a radial grid in order to implement exterior complex scaling. Thus, we expand the scattered wave functions that solve Eqs. (3) and (4) in partial waves of the form

$$\Psi^{\rm sc} = \sum_{l_1 m_1} \sum_{l_2 m_2} \frac{1}{r_1 r_2} \psi_{l_1 m_1, l_2 m_2}(r_1, r_2) Y_{l_1 m_1}(\hat{\mathbf{r}}_1) Y_{l_2 m_2}(\hat{\mathbf{r}}_2), \tag{8}$$

For both $\Psi_1^{\rm sc}$ and $\Psi_2^{\rm sc}$. This sum, in the case of $\Psi_1^{\rm sc}$ is over lm-pair configurations that give an overall $L = 1, M = 0$ state required by photoabsorbtion selection rules, while for $\Psi_2^{\rm sc}$ the lm-pairs are those that contribute to $L = 0, M = 0$ and $L = 2, M = 0$. The radial function $\psi_{l_1 m_1, l_2 m_2}(r_1, r_2)$ multiplying the product of spherical harmonics is taken to be a two-dimensional finite element-discrete variable representation (FEM-DVR) function, as in references [35] and [34]. The FEM-DVR radial basis is an attractive choice because of the computational efficiency gained as well as its natural complementarity for implementing exterior complex scaling [36].

In these calculations we used values of l_1 and l_2 up to 9, giving 228 (l_1, m_1, l_2, m_2) configurations. The ECS contour for each radial distance spanned along the real axis from the origin to $R_0 = 160\, a_0$, and extend in the complex plane to $R_{\rm max} = 230\, a_0$. The numerical grid was constructed from 17 finite elements along the real portion of the ECS contour and an additional 4 elements on the complex part, with each element using 18th order DVR. This leads to an overall linear system size of $n \sim 2.9 \times 10^7$.

The expansion of $\Psi_2^{\rm sc}$ in Eq. (8) leads naturally to a definition of partial wave amplitudes $\mathcal{F}_{l_1, l_2, m_1, m_2}(k_1, k_2)$ for ionization in terms of which the overall double ionization amplitude can be written [34]

$$f(\mathbf{k}_1, \mathbf{k}_2, \omega) = \sum_{l_1, m_1} \sum_{l_2, m_2} \left(\frac{2}{\pi}\right) i^{-(l_1+l_2)} e^{i\eta_{l_1}(k_1) + i\eta_{l_2}(k_2)} \times \Big[\mathcal{F}_{l_1, l_2, m_1, m_2}(k_1, k_2) Y_{l_1 m_1}(\hat{\mathbf{k}}_1) Y_{l_2 m_2}(\hat{\mathbf{k}}_2)\Big], \tag{9}$$

where $\eta_l(k)$ is a Coulomb phase shift. It is the partial wave amplitudes that we extrapolate from complex values of ω to $\mathrm{Im}[\omega] = 0$. in order to complete our calculation of the physical amplitudes and cross sections reported in the following discussion.

For each energy sharing, (k_1, k_2), we wish to consider, we evaluate $\mathcal{F}^{\gamma}_{l_1, l_2, m_1, m_2}(k_1, k_2)$ using $\Psi_2^{\rm sc}$ computed with $\mathrm{Im}[\omega] = \gamma$ for each configuration (l_1, l_2, m_1, m_2). The amplitude evaluation is done for a number of values of γ in the range $[\gamma_{\rm min} - \gamma_{\rm max}]$. In the current calculation $\gamma_{\rm max} = 0.500$ and $\gamma_{\rm min}$ in the range $[0.050 - 0.150]$ depending on the photon energy. Calculations with smaller values of γ become impractical since they require substantially larger grids for convergence. Each amplitude was then fit to a cubic polynomial in γ and the value of the polynomial at $\gamma = 0$ was the used as the value of $\mathcal{F}_{l_1, l_2, m_1, m_2}(k_1, k_2)$.

The *converged* real and imaginary parts of all the partial wave amplitudes were found to be smooth functions of $\mathrm{Im}[\omega] = \gamma$ and, with exceptions to be noted below, vary slowly as γ approaches zero. For small values of γ, depending on the photon energy and the energy sharing, the results depend on the size of the FEM-DVR grid, since the larger grids imply denser sets of discrete energy eigenvalues of the discretized Hamiltonian. For every photon energy considered the amplitudes were examined to identify the minimum value of γ to which a smooth cubic polynomial fit of the amplitude could be extended.

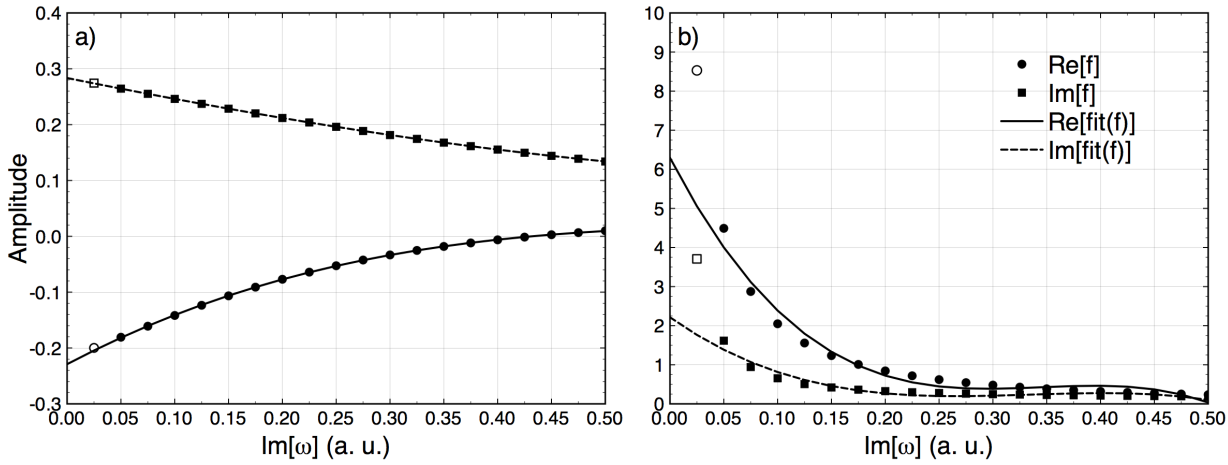

FIG. 1: Extrapolation to $\mathrm{Im}[\omega] = 0$ of real and imaginary parts of the ionization amplitude of Eq. (9), in atomic units. Left: $\mathcal{F}_{0,0,0,0}(k_1, k_2)$ with 40% energy sharing for a photon energy of 58 eV. Right: $\mathcal{F}_{1,0,1,0}(k_1, k_2)$ with 10% energy sharing. The open circles and squares mark calculated values that were not included in the cubic polynomial fits shown by the solid and dashed lines.

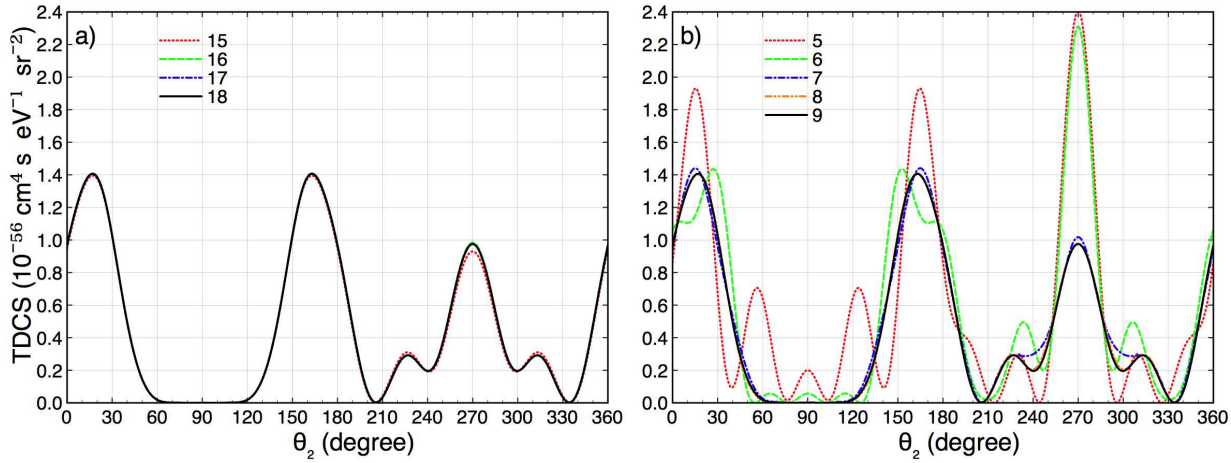

FIG. 2: Color online. Left convergence of TDCS at 46 eV and equal energy sharing for ejection of one electron at 90° to the polarization direction with respect to the order of the DVR basis in each finite element. Right: Convergence with respect to the maximum angular momentum included.

We have observed that the errors associated with extrapolating the amplitudes to real ω increase as we approach the threshold for sequential ionization. Examples of the extrapolation procedure are shown in Fig. 1 for a photon energy of 58 eV, which is above the sequential ionization threshold. For 40% energy sharing, where nonsequential ionization dominates, the amplitudes for both electrons ejected as s-waves are well fit by a cubic polynomial. This is not the case for simultaneous p-wave ejection at 10% energy sharing, where sequential ionization dominates, as seen by the behavior plotted in the right panel of Fig. 1. There is evidently substantial curvature in the amplitudes at small values of $\mathrm{Im}[\omega]$ which is difficult to capture with calculations that stop at $\mathrm{Im}[\omega] = 0.05$. This behavior is not surprising since, as we have previously pointed out [21] (see Appendix A), the two-photon double ionization amplitude is formally divergent above 54.4 eV at the energy sharings corresponding to sequential ionization. As the threshold for sequential ejection is approached from below, the amplitudes that dominate the cross section above that threshold begin to increase rapidly at extreme unequal energy sharings. That is the origin of the effect we have called "virtual sequential ionization" [21, 22]. In these regions our extrapolation procedure has the most error. Therefore, when we discuss the total cross section below we will attempt to estimate that error. However it appears that the resulting TDCS behavior remains qualitatively cor-

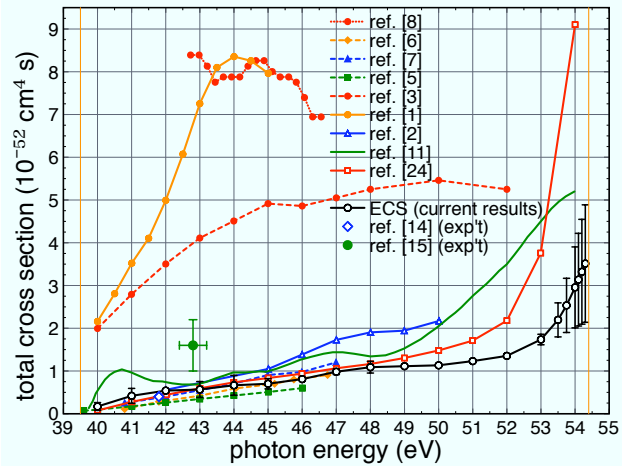

FIG. 3: (Color online) Total two-photon double ionization cross section.

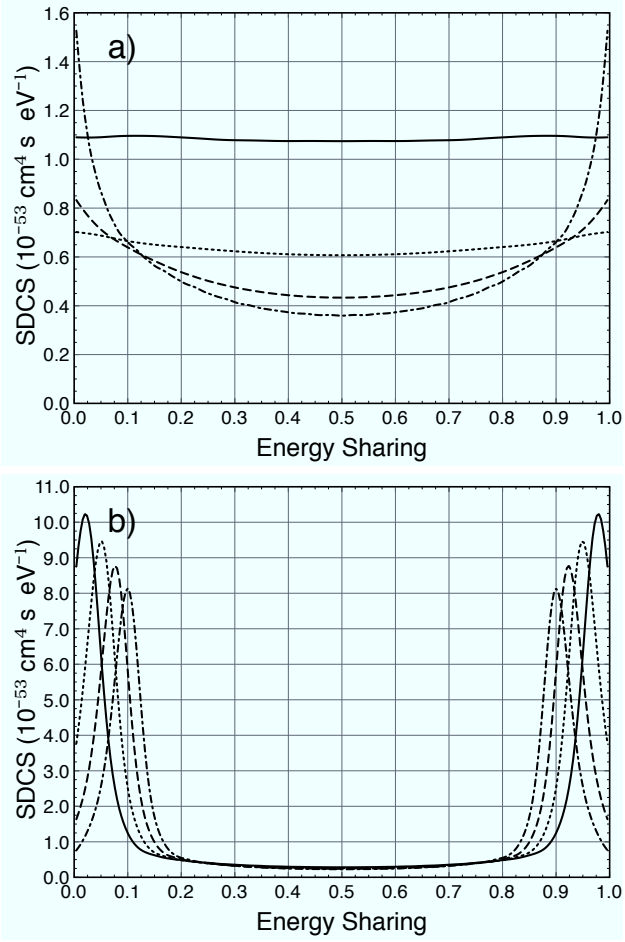

FIG. 4: a) SDCS for photon energies of 42, 45, 50, and 52 eV (solid, short dash, long dash, and dash-dot curves respectively). b) SDCS for photon energies of 55, 56, 57, and 58 eV (solid, short dash, long dash, and dash-dot curves respectively).

rect although there is some error in absolute magnitude. Near equal energy sharing that effect is minimized.

The calculations here involve a different extrapolation from those in ref. [21] where the cross sections, and not the individual partial wave amplitudes, were extrapolated from complex values of ω. The nuclear recoil cross sections presented very recently in ref. [22], on the other hand, did involve the extrapolation of the amplitudes since they depend on the TDCS. We emphasize that in the calculations we present here, convergence has been reached with respect to the number of angular momentum pairs (l_1, l_2, m_1, m_2) and the radial grids. That fact is demonstrated in Fig. 2 which shows the convergence of the TDCS for a case where its magnitude is smallest, namely when one electron is ejected perpendicular to the polarization direction. Thus we see that essentially all of the residual error originates in the extrapolation of Im$[\omega]$.

III. CROSS SECTIONS FOR TWO-PHOTON DOUBLE IONIZATION OF HELIUM

A. Integral cross section

In Fig. 3 we show the results of the present calculations for the total cross section computed from the extrapolated partial wave amplitudes together with a representative sampling of other calculations of this quantity. Several of the calculations shown in this figure are described by their authors as either explicitly or implicitly including correlation in the initial and final states and be able in principle to converge to an essentially exact result. Those include the Time-dependent Close Coupling (TDCC) results of Hu, Colgan and Collins [5], the TDCC results of Feist et al. [24], and the numerical time-dependent Schrödinger equation (TDSE) calculations of Piraux et al. [7] in all of these cases the ionizing wave packets are solutions of the TDSE, even though the amplitudes may be extracted by projection onto uncorrelated products of Coulomb continuum functions for each electron. The correlated treatments also include R-matrix Floquet calculations of Feng and van der Hart [6], and the second order quasi-energy approach of Shakeshaft [11] which both evaluate the total ionization cross section by other means. Below 50 eV agreement of the present results with all of those calculations is generally within a factor of 1.5 except very near threshold. We conclude that the differences are primarily due to various degrees of numerical error in the description of the wave functions. The present results are also in similar agreement with the convergent close-coupling (CCC) calculation of Ivanov and Kheifets [37] , which employed an additional closure approximation.

The rise in the total cross section as the sequential threshold is approached, seen in our earlier study [21] and subsequently verified by other investigators [11, 24],

is part of the effect we have called virtual sequential ionization. Above that threshold, the total cross section is formally infinite in lowest order perturbation theory. Between 50 eV and 54.4 eV, we note that the simple cubic polynomial fit to the partial wave amplitudes as functions of Im[ω] represents their behavior less well than at lower photon energies. In that region we have assigned error bars to our results based on varying γ_{min} in the range of extrapolation values, Im[ω] = [$\gamma_{\rm min} - \gamma_{\rm max}$] between 0.05 and 0.1 hartrees.

We find that for photon energies above 50 eV, while the magnitudes of the cross sections have some uncertainty due to the extrapolation procedure, the shapes of the angular distributions (the TDCS) do not vary significantly with the extrapolation parameters. Thus we conclude that the remaining disagreement in the total cross section and magnitudes of the other differential quantities that we calculate for those photon energies is due in part to a variation in the analytic behavior of the amplitudes for small values of Im[ω] that we do not capture correctly with this extrapolation procedure. However, the qualitative behaviors of the TDCS in that energy region and above the sequential threshold remains correct. Below 48 eV, our results seem to have converged unambiguously in all respects.

B. Single Differential Cross Sections

The calculated SDCS, defined as the integral of the TDCS over all directions of electron ejection,

$$\frac{d\sigma^{\rm SDCS}}{dE_1} = \int d\Omega_1 \int d\Omega_2 \frac{d\sigma}{dE_1 d\Omega_1 d\Omega_2} \qquad (10)$$

is shown for several energies below and above the sequential threshold in Fig. 4. At photon energies of 42 and 45 eV it is nearly flat as a function of energy sharing, E_1/E, where E is the photon energy minus the double ionization potential. Those cross sections above the sequential threshold show peaks at the energies for sequential ejection whose heights are formally infinite in this time-independent calculation of the lowest order perturbation theory description of photoejection. They have finite heights in these calculations as a result of the error inherent in the extrapolation procedure, which in turn has its origins in the finite size of the numerical grids we employ.

The signature of the virtual sequential ionization effect is seen in at 50 and 52 eV in Fig. 4 where the SDCS turns up near extreme energy sharing fractions. We have discussed previously how this behavior is essentially the appearance of the edges of the sequential peaks that appear above the sequential threshold [21, 22]. More specifically it can be attributed to the increasing contribution of the amplitudes for ejection of both electrons as p-waves.

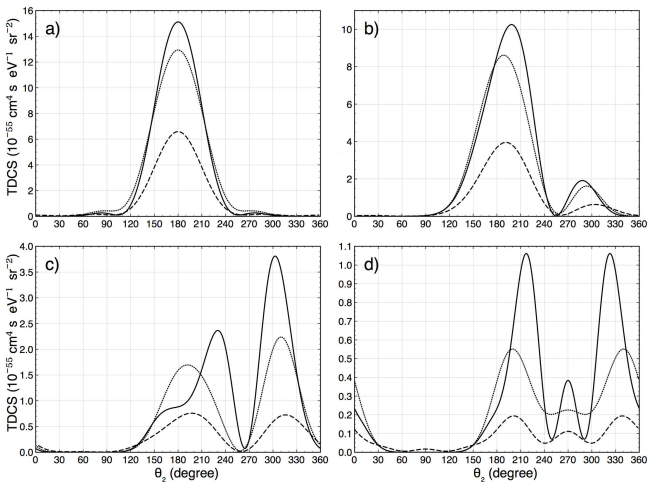

FIG. 5: TDCS for a photon energy of 42 eV with equal energy sharing. a) fixed electron at 0°, b) fixed electron at 30°. c) fixed electron at 60° and d) fixed electron at 90°. Solid curve: current result, dashed curve: TDCC calculations of ref. [5], dotted curve: TDCC calculations of ref.[24].

C. Triple Differential Cross Sections

The computed TDCS for a photon energy of 42eV and equal energy sharing is compared with the results of two previous time-dependent close-coupling calculations in Fig. 5. It is apparent from that comparison that some disagreement in magnitude remains between these completely *ab initio* calculations that is not resolved by scaling any of them by an overall constant, but that the shapes are generally in agreement. For equal energy sharing, the TDCS should be zero when both electrons exit in the same direction. This zero is a consequence of Coulomb repulsion, not a selection rule, and appears only in a completely converged calculation. These zeroes are reproduced to graphical accuracy in our ECS calculations and those of ref. [24] as well, while the TDCC calculations of ref. [5] give small but visible values in those directions.

Here we focus on an overview of the behavior of the TDCS and the way in which it reveals the presence of electron correlation and manifests virtual sequential ionization effects. To understand the qualitative behavior of the TDCS for two-photon ionization at any energy, and how it manifests effects that are due to electron correlation, it is essential to understand it first for sequential ionization where the effects of correlation are nearly negligible.

In Appendix A we sketch the derivation of the approximation to the amplitude for two-photon double ionization that we introduced in ref. [21], under a set of simplifying approximations that completely neglect both electron correlation and screening. It gives the following approx-

imation to the TDCS:

$$\frac{d\sigma^{\rm seq}}{dE_1 d\Omega_1 d\Omega_2} \approx \frac{\hbar}{4\pi}\left(\frac{3}{4\pi}\right)^2 \cos^2(\theta_1)\cos^2(\theta_2) \left(\frac{\sqrt{\sigma^{\rm He^+}(E_2)\sigma^{\rm He}(E_1)}}{E_0+\hbar\omega-\epsilon_{1s}-E_1} + \frac{\sqrt{\sigma^{\rm He^+}(E_1)\sigma^{\rm He}(E_2)}}{E_0+\hbar\omega-\epsilon_{1s}-E_2}\right)^2 . \tag{11}$$

In Eq.(11) $\sigma^{\rm He}(E)$ is the integral single ionization cross section of the neutral helium atom, and $\sigma^{\rm He^+}(E)$ is the exact integral single photoionization cross section of He^+. The key point here is that the angular dependence has the form of the product of two completely uncorrelated dipole distributions for the two electrons. We emphasize that Eq.(11) is a model for sequential ionization only in the sense that it is the simplest approximation to the second-order amplitude that captures its singularities at the ejection energies of the sequential process. More sophisticated treatments convert these singularities to peaks of finite height located at the same energies [38, 39].

If we integrate Eq.(11) over $d\Omega_1$ and $d\Omega_2$ we get the approximation to the SDCS used in reference [21] to qualitatively describe the origin of the sequential peaks:

$$\frac{d\sigma^{\rm seq}}{dE_1} \approx \frac{\hbar}{4\pi}\left(\frac{\sqrt{\sigma^{\rm He^+}(E_2)\sigma^{\rm He}(E_1)}}{E_0+\hbar\omega-\epsilon_{1s}-E_1} + \frac{\sqrt{\sigma^{\rm He^+}(E_1)\sigma^{\rm He}(E_2)}}{E_0+\hbar\omega-\epsilon_{1s}-E_2}\right)^2 . \tag{12}$$

With the understanding that the TDCS would be proportional to $\cos^2(\theta_1)\cos^2(\theta_2)$ for purely sequential ionization, we can turn our attention to Fig. 6, which shows the TDCS at two photon energies, plotted in three dimensions, for four directions of the fixed electron. At 58 eV for an energy sharing of 90%, which is close to the sequential peak of the SDCS, we see a dipole-like pattern apparently distorted by the interaction of the two outgoing electrons. The most dramatic effect is the almost complete extinction of the cross section when either electron is ejected at 90°, just as the $\cos^2(\theta_1)\cos^2(\theta_2)$ dependence of sequential ionization would suggest. In the same figure we see a similar plot for 46 eV photons and 50% energy sharing, in the purely nonsequential region, well away from the sequential threshold. It also is nearly extinguished when either electron is ejected perpendicular to the polarization direction, but at other angles of the fixed electron it is more strongly distorted from a simple dipole pattern.

We have found that at all energies below the sequential threshold and at all but very extreme energy sharing, the TDCS has the general behavior shown in the lower row of Fig. 6, suggesting a qualitative picture in which each electron is separately accelerated by the applied field. The TDCS is very small when either electron is ejected at angles nearly perpendicular to the polarization vector, a behavior very different from that of the TDCS for one-photon double ionization. For geometries that involve ejection perpendicular to the polarization vector, the TDCS is most difficult to converge in terms of the included angular momenta, underscoring the fact that it is in those geometries that the effects of electron correlation are most pronounced. Although the cross sections are very small in these geometries, as is seen for example in the rightmost case on the bottom row of Fig. 6, the ejection of an electron perpendicular to the polarization direction produces a more complicated angular pattern in the TDCS than at other geometries that is a signature of the electron correlation necessary for this process to take place.

Figure 7 demonstrates that in spite of the overall similarity of the shapes of the TDCS at different photon energies, it nevertheless shows the effect we call virtual sequential ionization below the sequential threshold. That figure shows the TDCS plotted as contour plots with respect to energy sharing and the ejection angle of one electron. As the energy is increased from 42 to 46 and to 52 eV we see the dominance of extreme energy sharings increase. The TDCS varies in magnitude with energy sharing showing a signature of the virtual sequential contribution, but its behavior with respect to angles varies more subtly with energy sharing as the sequential threshold is approached from below. At 56 eV, in the bottom row of that figure, the sequential peaks and the approximate $\cos^2(\theta_1)\cos^2(\theta_2)$ behavior is apparent.

D. Nuclear recoil cross sections

The momentum recoil, $\mathbf{Q}$, of the nucleus due to the ejection of two electrons of momenta $\mathbf{k}_1$ and $\mathbf{k}_2$ is

$$\mathbf{Q} = -(\mathbf{k}_1 + \mathbf{k}_2)\,. \tag{13}$$

The definition of the nuclear recoil cross section is thus given by the following integral of the SDCS.

$$\frac{d\sigma}{d^3\mathbf{Q}dE_1} = \int d\Omega_1 \int d\Omega_2 \, \frac{d\sigma}{d\Omega_1 d\Omega_2 dE_1}\, \delta^3(\mathbf{Q}+\mathbf{k}_1+\mathbf{k}_2)\,. \tag{14}$$

The delta function picks out $\mathbf{k}_1$ and $\mathbf{k}_2$ that are solutions to the set of equations,

$$\begin{aligned} \mathbf{Q} &= -(\mathbf{k}_1+\mathbf{k}_2) \\ |\mathbf{k}_1| &= k_1 \\ |\mathbf{k}_2| &= k_2\,. \end{aligned} \tag{15}$$

However, the numerical implementation of integral in Eq.(14) requires some effort because, for example, there are ranges in directions of $\mathbf{k}_1$, for which no $\mathbf{k}_2$ exists that satisfies Eq.(15). In Appendix B we give a simple algorithm with which to calculate $d\sigma/d^3\mathbf{Q}dE_1$, given the TDCS.

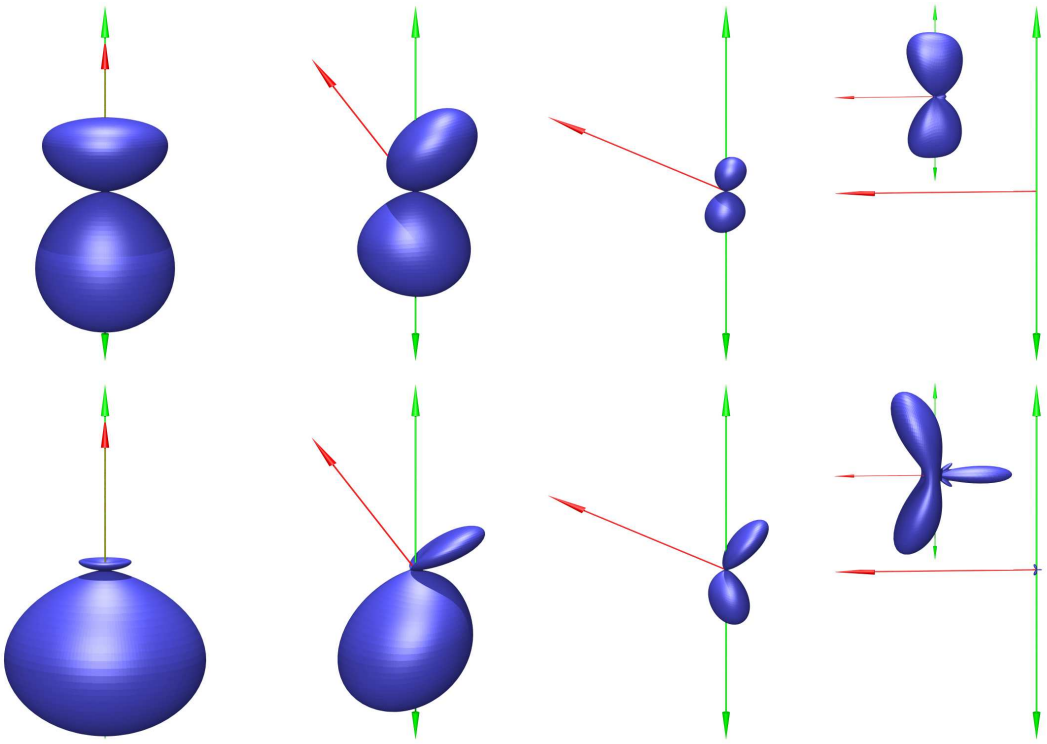

FIG. 6: Color online. Top: TDCS at 58 eV and 90% energy sharing for angles of the fixed electron (single headed arrow) of 0°, 30°, 60° and 90° from the polarization direction (double headed arrow). Bottom: same at 46 eV and 50% energy sharing. Inset in last column shows the cross section magnified 100 (top) and 40 (bottom) times.

The nuclear recoil can be measured directly in double ionization experiments using the COLTRIMS method, for example. Such observations do not require detection of the electrons at all, and thus avoid completely the need for coincidence measurements [16]. Nonetheless, this integrated quantity can show clear signatures of the sequential and nonsequential processes in two-photon double ionization as we have discussed previously [22]. Such a measurement integrates the differential nuclear recoil cross section in Eq.(14) over energy sharing, and sometimes over one component of the recoil momentum, $\mathbf{Q}$. It is interesting to see the how the nuclear recoil behaves in more detail, as a function of energy sharing, for example, although the measurement of the fully differential quantity requires a coincidence measurement.

In Fig. 8 we show a cut of the momentum recoil plane with $Q_y = 0$ for energy sharings of 10% and 45% for one photon energy above and and another below the sequential ionization threshold. The far right hand panels of that figure shows the prediction of the simple model in Eq.(11). At 58 eV, comparison with the full ECS calculations in the same figure shows that the simple model, which completely neglects any correlation between the electrons as well as electrostatic shielding, agrees almost perfectly in its qualitative behavior with the full calculations. That comparison suggests that the effects of electron correlation, even at near equal energy sharing, are almost obscured in the nuclear recoil cross section by the dominance of the sequential process at photon energies where it can take place.

On the other hand at a photon energy of 42 eV, far below the sequential threshold, the nuclear recoil cross section does in fact reflect some of the behavior of the underlying TDCS when it is plotted for specific energy sharings, as is shown in the leftmost panels of Fig. 8. The integration over the ranges of angles described in Appendix B does however obscure much of that detail, so that at these energies where only the nonsequential process is possible the features that remain in the nuclear recoil cross section largely reflect the combination of the energy sharing probabilities and the conservation of momentum. These conclusions also apply to the cross sections integrated over Q_y that are shown in Fig. 9. Although the shapes of the recoil patterns change somewhat the main features remain similar.

We can conclude that while observing the nuclear recoil cross section, even integrated over energy sharings, reveals some of the kinematics of the double ionization process, only a kinematically complete experiment, measuring the momenta of either both electrons or one electron and the nucleus, carries the detail of the TDCS necessary to reveal the effects of electron dynamics and the details of double photoejection dynamics.

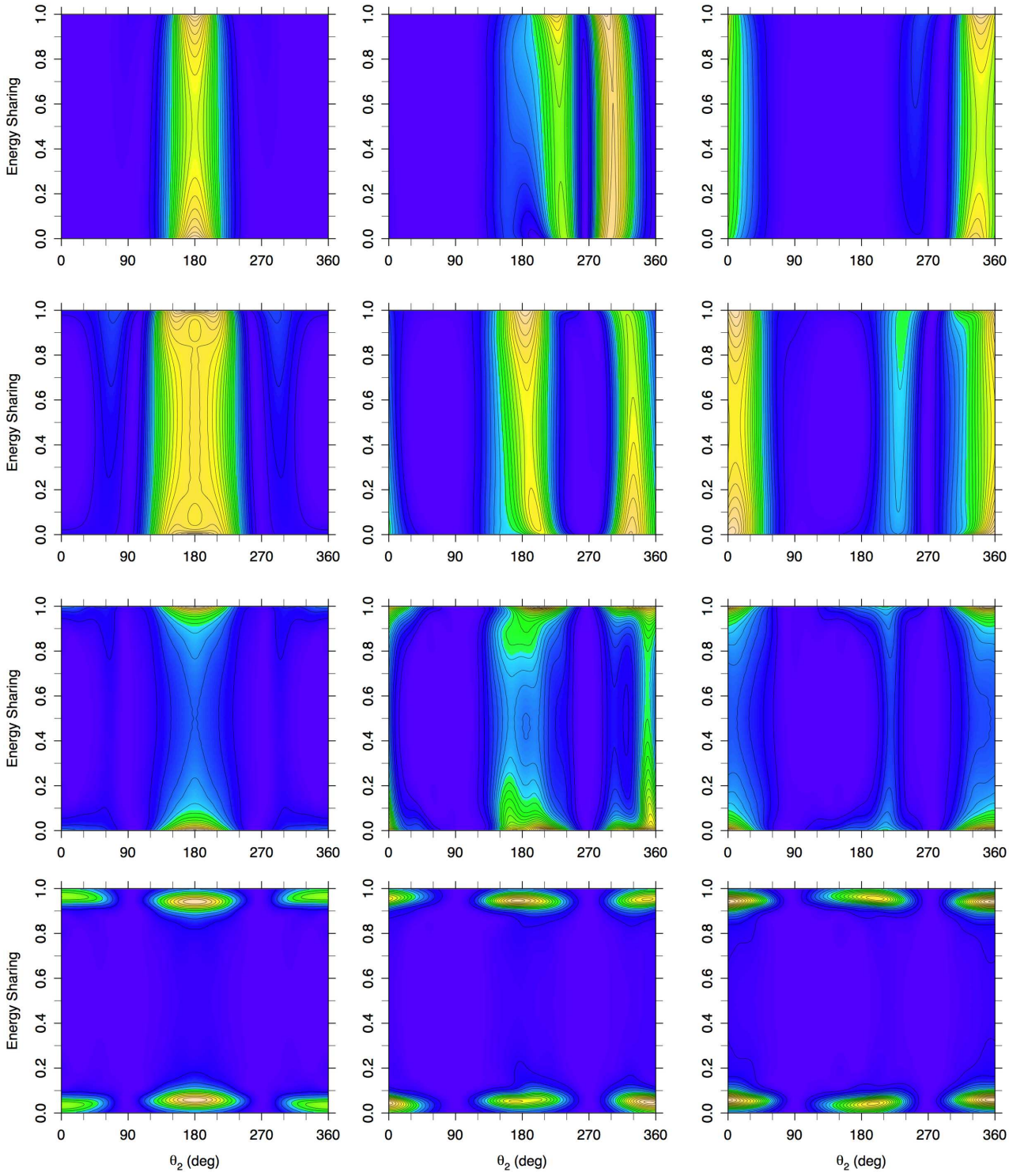

FIG. 7: Color online. Contour plot of triple differential cross section for various energy sharings for photon energies of (top to bottom) 42, 46, 52 and 56 eV. The angle, θ_1 of the fixed electron is (left to right) 0°, 60° and 150°.

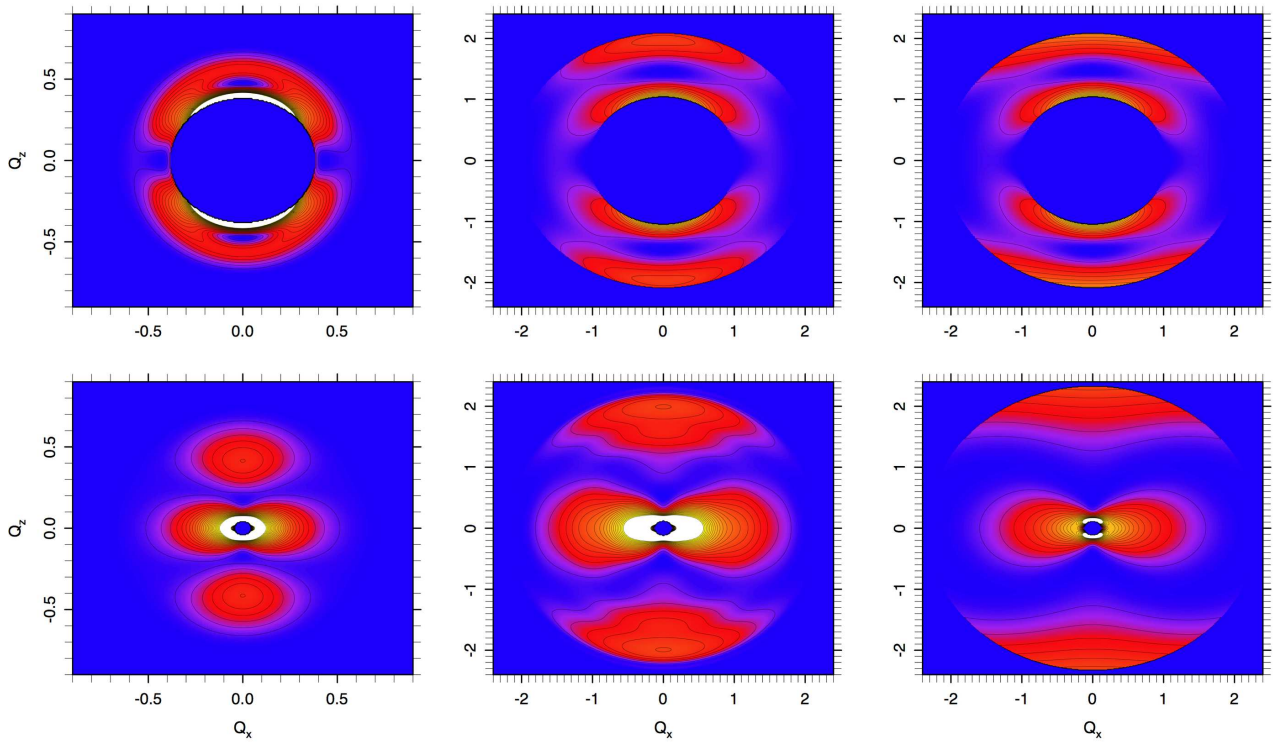

FIG. 8: Color online. Nuclear recoil cross sections in with $Q_y = 0$ (with Q_z in the direction of polarization) for (columns, left to right) 42 eV, 58 eV and the sequential model at 58 eV. $\mathbf{Q}$ in atomic units. Top row is 10% and and bottom row is 45% energy sharing.

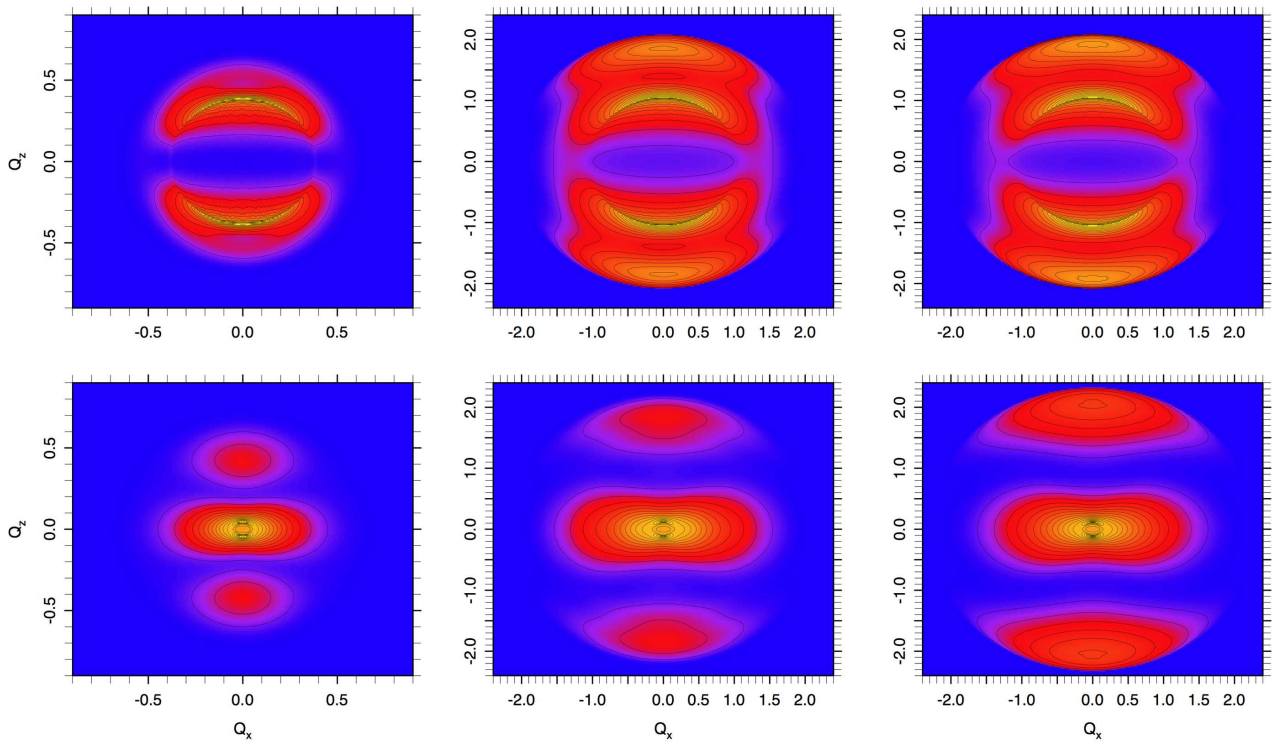

FIG. 9: Color online. Same as Fig. 8, integrated over Q_y

IV. CONCLUSION

In this study we have presented a complete description of the two-photon double photoionization of helium from a time-independent implementation of the lowest order perturbation theory equations for the process. The combination of ECS and the grid methods we have used in other contexts can solve those equations accurately, converging the solution with respect to partial waves and the spatial basis of DVR functions. Because the driving term of the second of those equations does not limit to zero as the coordinates of either electron go to infinity it was necessary to employ extrapolation from complex values of the photon frequency in its solution. This computational device has not been necessary in any previous application of the ECS method to multiple photoionization or electron-impact ionization.

A complete picture of the dynamics of two-photon double ionization has emerged from these calculations. In the SDCS the effects of "virtual sequential ionization," which are the wings of the peaks that appear above the sequential threshold, are clearly visible above a photon energy of 50 eV. The rise in the total cross section as the sequential threshold is approached is due to this effect.

A global overview of the angular dependence of double photoejection by two photons produced in these calculations is instructive. While the effects of electron correlation are dramatically visible in the TDCS for some ejection geometries, a qualitative signature of the separate acceleration of the two electrons by the field persists at energies where only nonsequential absorption of the two photons is possible. The TDCS for the range of energies from 42 eV to 54.4 eV can be understood qualitatively as a modification by the effects of electron correlation and final state interaction of the simple $\cos^2(\theta_1)\cos^2(\theta_2)$ pattern which would be present for sequential ionization. A consideration of the details of the nuclear recoil cross sections, not integrated over energy sharing, reveals that this quantity reflects primarily the energetics of the double ejection process and shows only subtle suggestions of the details of the TDCS that carry information about electron correlation.

These observations forcefully underscore the need for detailed, kinematically complete experiments to unravel the details of the correlated dynamics of multiple photoionization, for either continuous wave radiation or in emerging ultrafast time resolved studies.

Acknowledgments

This work was performed under the auspices of the US Department of Energy by the University of California Lawrence Berkeley National Laboratory under Contract

DE-AC02-05CH11231 and the Los Alamos National Laboratory under Contract DE-AC52-06NA25396 and was was supported by the U.S. DOE Office of Basic Energy Sciences, Division of Chemical Sciences. CWM acknowledges support from the National Science Foundation (Grant No. PHY-0604628). Computations were carried out using the Institutional Computing resources at LANL.

Appendix A: Approximate treatment of two-photon double ionization in the vicinity of the sequential threshold

We begin with the definition of the cross section for two-photon double ionization in the velocity form given in Eqs.(1) and (2). To find the contribution for sequential ionization we focus only on the contribution to the Green's function of the single ionized intermediate states in which the He^+ is left in its ground state, neglecting the contribution of intermediate bound and doubly ionized states to the resolvent. We thus approximate the matrix element of the resolvent that appears in Eq.(2) by

$$\langle \Psi^-_{\mathbf{k}_1,\mathbf{k}_2}|\mu[E_0+\hbar\omega-H+i\epsilon]^{-1}\mu|\Phi_0\rangle \approx \int d^3\mathbf{k}_0 \frac{\langle \Psi^-_{\mathbf{k}_1\mathbf{k}_2}|\mu|\psi^-_{\mathbf{k}_0,1s}\rangle\langle\psi^-_{\mathbf{k}_0,1s}|\mu|\Phi_0\rangle}{E_0+\hbar\omega-\epsilon_{1s}-k_0^2/2+i\eta} \quad \text{(A1)}$$

where ϵ_{1s} is the ground state energy He^+, and as before $\mu=\boldsymbol{\epsilon}\cdot\mathbf{p}_1+\boldsymbol{\epsilon}\cdot\mathbf{p}_2$ is the velocity form of the dipole operator.

The matrix element $\langle\psi^-_{\mathbf{k}_0,1s}|\mu|\Phi_0\rangle$ can immediately be recognized as the amplitude for one-photon single ionization of He, but to proceed we need an approximation to the other integral in the numerator of this expression

$$\langle \Psi^-_{\mathbf{k}_1\mathbf{k}_2}|\mu|\psi^-_{\mathbf{k}_0,1s}\rangle = \langle \Psi^-_{\mathbf{k}_1\mathbf{k}_2}|\boldsymbol{\epsilon}\cdot\mathbf{p}_1+\boldsymbol{\epsilon}\cdot\mathbf{p}_2|\psi^-_{\mathbf{k}_0,1s}\rangle \quad \text{(A2)}$$

To approximate this matrix element we make the following two simplifying assumptions:

1. Ignore final state interaction completely so we can write the final state as a symmetrized product of Coulomb functions with charge $Z=2$,

$$\Psi^-_{\mathbf{k}_1\mathbf{k}_2}(\mathbf{r}_1,\mathbf{r}_2) \approx \mathcal{P}\{\varphi^{Z=2(-)}_{\mathbf{k}_1}(\mathbf{r}_1)\quad \varphi^{Z=2(-)}_{\mathbf{k}_2}(\mathbf{r}_2)\} \quad \text{(A3)}$$

   where $\mathcal{P}=1/\sqrt{2}(1+P_{12})$ is the symmetrizer (the intermediate states are all singlets) so that this wave function has delta function normalization in momentum ($\delta(\mathbf{k}_1-\mathbf{k}'_1)\delta(\mathbf{k}_2-\mathbf{k}'_2)$).

2. Ignore any correlation in $\psi^-_{\mathbf{k}_0,1s}$, and ignore screening of the outgoing electron by the 1s electron in He^+,

$$\psi^-_{\mathbf{k}_0,1s} \approx \varphi^{Z=2(-)}_{\mathbf{k}_0}(\mathbf{r}_1)\varphi^{He^+}_{1s}(\mathbf{r}_2) \quad \text{(A4)}$$

With these approximations, the integral over $d^3\mathbf{k}_0$ in Eq.(A1) will be controlled by the delta function from the free-free overlap $\langle\varphi^{Z=2(-)}_{\mathbf{k}_1}|\varphi^{Z=2(-)}_{\mathbf{k}_0}\rangle = \delta(\mathbf{k}_1-\mathbf{k}_0)$ as pointed out in another context by Proulx, Pont and Shakeshaft [10]. So for the numerator matrix element in Eq.(A2) we have

$$\langle \Psi^-_{\mathbf{k}_1\mathbf{k}_2}|\mu|\psi^-_{\mathbf{k}_0,1s}\rangle = \frac{1}{\sqrt{2}}\Big(\delta(\mathbf{k}_1-\mathbf{k}_0)\langle\varphi^{Z=2(-)}_{\mathbf{k}_2}|\boldsymbol{\epsilon}\cdot\mathbf{p}|\varphi^{He^+}_{1s}\rangle + \delta(\mathbf{k}_2-\mathbf{k}_0)\langle\varphi^{Z=2(-)}_{\mathbf{k}_1}|\boldsymbol{\epsilon}\cdot\mathbf{p}|\varphi^{He^+}_{1s}\rangle\Big). \quad \text{(A5)}$$

With these approximations, Eqs.(A1), (1) and (2) give the sequential contribution to the TDCS as

$$\frac{d\sigma^{seq}}{dE_1 d\Omega_1 d\Omega_2} \approx \frac{2\pi}{\hbar}(2\pi\alpha)^2\frac{1}{m^2\omega^2}k_1k_2 \times\frac{1}{2}\left|\frac{\langle\varphi^{Z=2(-)}_{\mathbf{k}_2}|\boldsymbol{\epsilon}\cdot\mathbf{p}|\varphi^{He^+}_{1s}\rangle\langle\psi^-_{\mathbf{k}_1,1s}|\mu|\Phi_0\rangle}{E_0+\hbar\omega-\epsilon_{1s}-k_1^2/2} + \frac{\langle\varphi^{Z=2(-)}_{\mathbf{k}_1}|\boldsymbol{\epsilon}\cdot\mathbf{p}|\varphi^{He^+}_{1s}\rangle\langle\psi^-_{\mathbf{k}_2,1s}|\mu|\Phi_0\rangle}{E_0+\hbar\omega-\epsilon_{1s}-k_2^2/2}\right|^2. \quad \text{(A6)}$$

The quantities in numerators of Eq.(A6) can be simply related to the cross sections for single photoionization of He and He^+. For example, the cross section for the one-photon ionization of He is given in this gauge by

$$\frac{d\sigma}{d\Omega} = \frac{(2\pi)^2 k\alpha}{\hbar\omega m}|\langle\psi^-_{\mathbf{k},1s}|\mu|\Phi_0\rangle|^2 \quad \text{(A7)}$$

and the cross section for ionization of He^+ is given by the same formula with the amplitude $\langle\varphi^{Z=2(-)}_{\mathbf{k}_1}|\boldsymbol{\epsilon}\cdot\mathbf{p}|\varphi^{He^+}_{1s}\rangle$. If we ignore the phases of these amplitudes, we can approximate the matrix elements in Eq.(A6) as

$$\langle\psi^-_{\mathbf{k},1s}|\mu|\Phi_0\rangle = \left(\frac{\hbar\omega m}{(2\pi)^2 k\alpha}\frac{d\sigma}{d\Omega}\right)^{1/2} = \left(\frac{\hbar\omega m}{(2\pi)^2 k\alpha}\frac{\sigma^{He}(E)}{4\pi}(1+\beta^{He}(E)P_2(\cos(\theta)))\right)^{1/2} \quad \text{(A8)}$$

and with an analogous formula for the other amplitude, $\langle\varphi^{Z=2(-)}_{\mathbf{k}}|\boldsymbol{\epsilon}\cdot\mathbf{p}|\varphi^{He^+}_{1s}\rangle$. In the present case, both of these are simple s to p transitions, so $\beta=2$ and $(1+\beta P_2(\cos(\theta)) = 3\cos^2(\theta)$.

Substituting Eq.(A8) and its analogue for $\langle\varphi^{Z=2(-)}_{\mathbf{k}}|\boldsymbol{\epsilon}\cdot\mathbf{p}|\varphi^{He^+}_{1s}\rangle$ into Eq(A6) gives the simple result for the TDCS in Eq.(11). This approximate result can be further generalized to the sequential ionization of initial states of other symmetries, but in those cases the energy dependence of the β parameters must also be considered.

Appendix B: Calculation of nuclear recoil cross section

Here we give a simple algorithm for computing the nuclear recoil cross section of Eq.(14). For an atom, no matter the direction of the polarization vector, $\boldsymbol{\epsilon}$, we can choose the z axis to lie along $\mathbf{Q}$ for the purpose of the integrations over Ω_1 and Ω_2 in Eq.(14). In that coordinate system we can solve the geometry problem for finding the set of $\mathbf{k}_1$ and $\mathbf{k}_2$ vectors that will sum to $\mathbf{Q}$. Those vectors make the angles θ_1 and θ_2 respectively with $\mathbf{Q}$

$$\cos(\theta_1) = \frac{Q^2 + k_1^2 - k_2^2}{2Qk_1} \tag{B1}$$

$$\cos(\theta_2) = \frac{Q^2 + k_2^2 - k_1^2}{2Qk_2} \tag{B2}$$

$$\phi_1 = \phi_2 + \pi \tag{B3}$$

where ϕ_1 and ϕ_2 are the the other spherical polar angles angles of $\mathbf{k}_1$ and $\mathbf{k}_2$ around $\mathbf{Q}$. Note also that

$$k_1 \sin(\theta_1) = k_2 \sin(\theta_2)\,. \tag{B4}$$

The task of computing the nuclear recoil cross section requires performing the four integrals in Eq.(14) over the angles specifying the directions of $\mathbf{k}_1$ and $\mathbf{k}_2$ (namely θ_1, θ_2, ϕ_1, and ϕ_2) while making use of the delta function to perform three of them. Using $\mathbf{Q}$ as the z axis of our coordinate system for the definition of θ_1, θ_2, ϕ_1, and ϕ_2 allows us to rewrite the delta function $\delta(\mathbf{Q} + \mathbf{k}_1 + \mathbf{k}_2) = \delta(Q_x + k_{1x} + k_{2x})\delta(Q_y + k_{1y} + k_{2y})\delta(Q_z + k_{1z} + k_{2z})$ in terms of these angles and convert the integral in Eq.(14) to the form

$$\frac{d\sigma}{d^3\mathbf{Q}dE_1} = \int\int\int\int \frac{d\sigma}{d\Omega_1 d\Omega_2 dE_1} \frac{\delta(\theta_1 - \theta_{1Q})\delta(\theta_2 - \theta_{2Q})\delta(\phi_1 - \phi_2 - \pi)}{\left|\frac{\partial(Q_x,Q_y,Q_z}{\partial(\theta_1,\theta_2,\phi_1}\right|} \sin\theta_1 d\theta_1 d\phi_1 \sin\theta_2 d\theta_2 d\phi_2\,. \tag{B5}$$

In Eq.(B5) $\left|\frac{\partial(Q_x,Q_y,Q_z}{\partial(\theta_1,\theta_2,\phi_1}\right|$ is the 3×3 Jacobian of the transformation between Q_x, Q_y, Q_z and $\theta_1, \theta_2, \phi_1$,

$$-Q_x = k_1 \sin\theta_1 \cos\phi_1 + k_2 \sin\theta_2 \cos\phi_2 \tag{B6}$$

$$-Q_y = k_1 \sin\theta_1 \sin\phi_1 + k_2 \sin\theta_2 \sin\phi_2 \tag{B7}$$

$$-Q_z = k_1 \cos\theta_1 + k_2 \cos\theta_2\,. \tag{B8}$$

We can simplify that determinant to

$$\left|\frac{\partial(Q_x, Q_y, Q_z}{\partial(\theta_1, \theta_2, \phi_1)}\right| = k_1^2 k_2 \sin\theta_1 \sin(\theta_1 + \theta_2)\,. \tag{B9}$$

Some additional algebra making use of Eqs.(B1), (B2), (B3) and (B4) shows that

$$\frac{\sin\theta_2}{k_1^2 k_2 \sin(\theta_1 + \theta_2)} = \frac{1}{Qk_1k_2} \tag{B10}$$

yielding the final result for the integral in Eq.(B5) with $\mathbf{Q}$ as the z axis

$$\frac{d\sigma}{d^3\mathbf{Q}dE_1} = \int_0^{2\pi} \frac{d\phi_2}{Qk_1k_2} \left(\frac{d\sigma}{d\Omega_1 d\Omega_2 dE_1}\right) \tag{B11}$$

with the angles θ_1, θ_2 and ϕ_1 at which the TDCS is evaluated in the integrand being determined by Eqs.(B1), (B2) and (B3).

Eq.(B11) produces the nuclear recoil cross section, but to comparison with experiment we must take the further step of expressing the result in terms of the components of $\mathbf{Q}$ in a coordinate system in which the polarization vector $\boldsymbol{\epsilon}$ lies along the z axis. Since we compute the TDCS, $d\sigma/d\Omega_1 d\Omega_2 dE_1$, with the angles expressed in that coordinate system (as in Eq.(11) for example), this is an easy task.

So to accumulate the integral in Eq.(B11) numerically we follow the following algorithm:

1. Pick a ϕ_2 quadrature point in Eq.(B11) .
2. Calculate θ_1 , θ_2 and ϕ_1 via Eqs.(B1), (B2) and (B3).
3. Transform those angles to angles with respect to a coordinate system with $\boldsymbol{\epsilon}$ as the z axis.
4. Evaluate TDCS in that coordinate system.
5. Accumulate sum for the numerical quadrature over ϕ_2.
6. Go to 1.

[1] L. A. A. Nikolopoulos and P. Lambropoulos, J. Phys. B **40**, 1347 (2007).
[2] I. A. Ivanov and A. S. Kheifets, Phys. Rev. A **75**, 033411 (2007).
[3] E. Foumouo, G. L. Kamta, G. Edah, and B. Piraux, Phys. Rev. A **74**, 063409 (2006).
[4] A. S. Kheifets and I. A. Ivanov, J. Phys. B **39**, 1731 (2006).
[5] S. X. Hu, J. Colgan, and L. A. Collins, J. Phys. B **38**, L35 (2005).
[6] L. Feng and H. W. van der Hart, J. Phys. B **36**, L1 (2003).

[7] B. Piraux, J. Bauer, S. Laulan, and H. Bachau, Eur. Phys. J. D **26**, 7 (2003).

[8] L. A. A. Nikolopoulos and P. Lambropoulos, J. Phys. B **34**, 545 (2001).

[9] J. Colgan and M. S. Pindzola, Phys. Rev. Lett. **88**, 173002 (2002).

[10] D. Proulx, M. Pont, and R. Shakeshaft, Phys. Rev. A **49**, 1208 (1994).

[11] R. Shakeshaft, Phys. Rev. A **76**, 063405 (2007).

[12] E. Foumouo, P. Antoine, B. Piraux, L. Malegat, H. Bachau, and R. Shakeshaft, J. Phys. B: At. Mol. Opt. Phys. **41**, 1 (2008).

[13] E. Foumouo, P. Antoine, and H. B. B. Piraux, New Journal of Physics **10**, 025017 (2008).

[14] H. Hasegawa, E. J. Takahashi, Y. Nabekawa, K. L. Ishikawa, and K. Midorikawa, Phys. Rev. A **71**, 023407 (2005).

[15] A. A. Sorokin, M. Wellhöfer, S. V. Bobashev, K. Tiedtke, and M. Richter, Phys. Rev. A. **75**, 051402(R) (2007).

[16] A. Rudenko, *et al.*, Phys. Rev. Lett. **101**, 073003 (2008).

[17] V. Ayvazyan, *et al.*, Eur. Phys. J. D **37**, 297 (2006).

[18] T. Sekikawa, A. Kosuge, T. Kanai, and S. Watanabe, Nature **432**, 605 (2004).

[19] O. Schwarzkopf, B. Krassig, J. Elmiger, and V. Schmidt, Phys. Rev. Lett. **70**, 3008 (1993).

[20] Th. Weber, *et al.*, Nature (London) **431**, 437 (2004).

[21] D. A. Horner, F. Morales, T. N. Rescigno, F. Martín, and C. W. McCurdy, Phys. Rev. A **76**, 030701(R) (2007).

[22] D. A. Horner, T. N. Rescigno, and C. W. McCurdy, Phys. Rev. A **77**, 030703(R) (2008).

[23] A. Dalgarno and J. T. Lewis, Proc. Roy. Soc. (London), Series A **233**, 70 (1955).

[24] J. Feist, S. Nagele, R. Pazourek, E. Persson, B. I. Schneider, L. A. Collins, and J. Burgdorfer, Phys. Rev. A. **77**, 043420 (2008).

[25] M. R. H. Rudge, Rev. Mod. Phys. **40**, 564 (1968).

[26] M. R. H. Rudge and M. J. Seaton, Proc. Roy. Soc. London **283**, 262 (1965).

[27] R. K. Peterkop, Opt. Spektrosk. **13**, 153 (1962) [Opt. Spectrosc. **13**, 87 (1962)].

[28] C. W. McCurdy, M. Baertschy, and T. N. Rescigno, J. Phys. B **37**, R137 (2004).

[29] C. W. McCurdy and T. N. Rescigno, Phys. Rev. A **62**, 032712 (2000).

[30] M. Baertschy, T. N. Rescigno, and C. W. McCurdy, Phys. Rev. A **64**, 022709 (2001).

[31] A. Palacios, C. W. McCurdy, and T. N. Rescigno, Phys. Rev. A **76**, 043420 (2007).

[32] T. N. Rescigno, M. Baertschy, W. A. Isaacs, and C. W. McCurdy, Science **286**, 2474 (1999).

[33] M. Baertschy, T. N. Rescigno, W. A. Isaacs, X. Li, and C. W. McCurdy, Phys. Rev. A **63**, 022712 (2001).

[34] F. L. Yip, D. A. Horner, C. W. McCurdy, and T. N. Rescigno, Phys. Rev. A **75**, 042715 (2007).

[35] D. A. Horner, W. Vanroose, T. N. Rescigno, F. Martín, and C. W. McCurdy, Phys. Rev. Lett. **98**, 073001 (2007).

[36] T. N. Rescigno and C. W. McCurdy, Phys. Rev. A **62**, 032706 (2000).

[37] A. S. Kheifets and I. A. Ivanov, J. Phys. B **39**, 1731 (2007).

[38] H. Bachau and P. Lambropoulos, Phys. Rev. A **44**, R9 (1991).

[39] M. A. Kornberg and P. Lambropoulos, J. Phys. B **32**, L603 (1999).